Terahertz Sum-Frequency Excitation of a Raman-Active Phonon

Sebastian Maehrlein,[1,*] Alexander Paarmann,[1] Martin Wolf,[1] and Tobias Kampfrath[1,2]

[1]*Department of Physical Chemistry, Fritz Haber Institute of the Max Planck Society, Faradayweg 4-6, 14195 Berlin, Germany*
[2]*Department of Physics, Freie Universität Berlin, Arnimallee 14, 14195 Berlin, Germany*

In stimulated Raman scattering, two incident optical waves induce a force oscillating at the difference of the two light frequencies. This process has enabled important applications such as the excitation and coherent control of phonons and magnons by femtosecond laser pulses. Here, we experimentally and theoretically demonstrate the so far neglected up-conversion counterpart of this process: THz sum-frequency excitation of a Raman-active phonon mode, which is tantamount to two-photon absorption by an optical transition between two adjacent vibrational levels. Coherent control of an optical lattice vibration of diamond is achieved by an intense terahertz pulse whose spectrum is centered at half the phonon frequency of 40 THz. Remarkably, the carrier-envelope phase of the THz pulse is directly transferred into the phase of the lattice vibration. New prospects in general infrared spectroscopy, action spectroscopy, and lattice trajectory control in the electronic ground state emerge.

Gaining control over ultrafast elementary motions of electrons, spins, and ions in solids is of major scientific and applied interest. Examples include steering of chemical reactions along a desired pathway [1] and switching of spins in magnetically ordered materials [2,3]. Many control strategies take advantage of terahertz (THz) modes of the material. An ubiquitous example is lattice vibrations (phonons) whose control by femtosecond laser pulses [4,5] has enabled new pathways to permanent material modification [6], insulator-to-metal transitions [7,8], and magnetization manipulation [2,9].

For selective excitation of coherent lattice vibrations, schemes based on one- or two-photon interactions are established [see Figs. 1(a) and 1(b)]. In the most straightforward approach, the laser electric field resonantly drives the electric dipoles of a long-wavelength lattice mode. This one-photon absorption (1PA) process requires an infrared-active transition and a pump spectrum that covers the phonon frequency $\Omega/2\pi$, typically between ~ 1 and 40 THz [Fig. 1(a)] [10–13]. To date, most works have implemented lattice excitation using stimulated Raman scattering (SRS) of a light pulse containing frequencies ω_1' and $\omega_2' = \omega_1' + \Omega$, both at roughly $2\pi \times 500$ THz [Fig. 1(b)]. The two rapidly oscillating light-field components couple primarily to electrons of the material [14], either nonresonantly (in optically transparent solids) [15,16] or resonantly (in opaque solids) [17,18], resulting in a force that coherently drives the lattice at the difference frequency $\omega_2' - \omega_1' = \Omega$. Such rectification can also be achieved through anharmonic interaction with resonantly driven infrared-active phonons at ω_1' and ω_2' [19].

Note that the difference-frequency process underlying SRS [Fig. 1(b)] is a familiar phenomenon in nonlinear optics where it is accompanied by the generation of sum-frequency signals [20]. This analogy suggests a novel scheme of coherent lattice control: the two incident frequencies are chosen such that their *sum* is resonant with the target mode [Fig. 1(c)]. Such sum-frequency excitation (SFE) by a single light pulse is tantamount to two-photon absorption (2PA) and offers similarly attractive features as 1PA. So far, 2PA has been widely used to induce [21,22] and coherently control [23,24] electronic transitions by ~ 1 eV photons. However, 2PA by vibrational resonances such as optical phonons has not yet been demonstrated because the laser frequencies used (~ 500 THz) were typically one order of magnitude larger than the highest phonon frequencies.

In this work, we provide a first experimental and theoretical demonstration of SFE of lattice vibrations. An intense THz pulse with a center frequency of 20 THz is found to coherently drive the long-wavelength Raman-active optical phonon of diamond at the sum frequency of 40 THz. Remarkably and similar to 1PA, the carrier-envelope phase (CEP) of the THz pulse is imprinted into the phase of the lattice vibration. Because of the low THz photon energy, parasitic electronic excitations are suppressed, thereby opening the way to coherent control of Raman-active modes such as phonons and magnons in the electronic ground state.

Experiment.—In our pump-probe scheme [Fig. 1(d)], a THz pump pulse with tunable center frequency [25] is directed onto the sample to drive coherent lattice vibrations. The instantaneous time-dependent phonon amplitude is monitored by a time-delayed optical probe pulse measuring the transient birefringence of the material [4,5].

As a sample, we choose a high-purity (100)-oriented diamond single crystal (type IIa, thickness 200 μm) grown by chemical vapor deposition. We focus on the zone-center F_{2g} optical phonon at $\Omega/2\pi \approx 40$ THz, which is one of the highest phonon frequencies known. This mode has a vanishing electric dipole moment but is strongly Raman
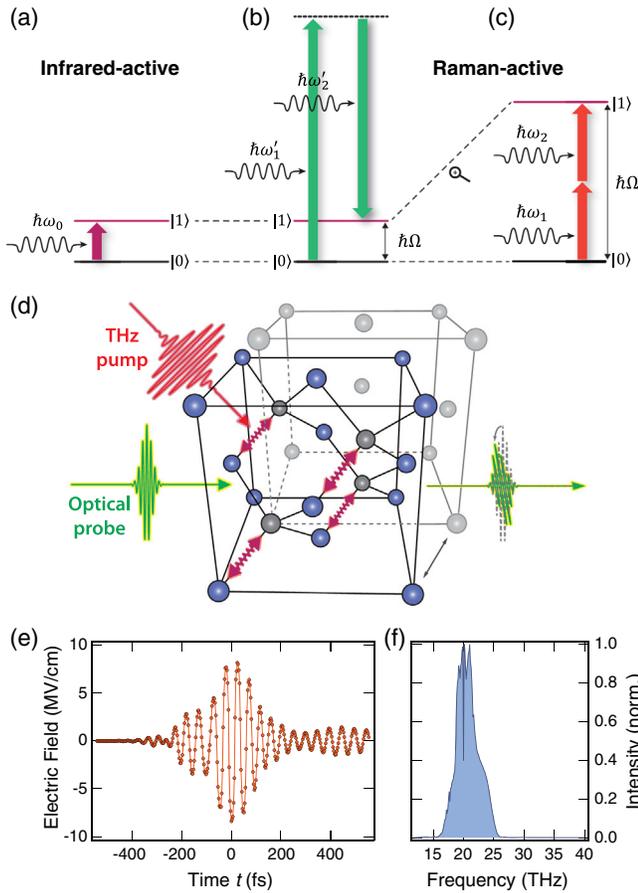
FIG. 1. (a)–(c) Schemes for driving coherent phonons.
(a) Direct excitation by one-photon absorption (1PA): the pump
frequency is resonant with the infrared-active phonon mode.
(b) Stimulated Raman scattering (SRS): the difference frequency
of two spectral components of the pump field is resonant with a
Raman-active phonon mode. (c) Sum-frequency excitation
(SFE): the sum frequency of two incident THz electric-field
components is resonant with a Raman-active phonon mode. This
process can be considered as two-photon absorption (2PA) by an
optical transition between two adjacent vibrational levels. (d) Unit
cell of diamond and schematic of the experiment: an intense THz
pulse (red) excites the F_{2g} mode whose dynamics are monitored
by a delayed ultrashort optical probe pulse (green). Red arrows
indicate coherent lattice motion corresponding to the Raman-
active, infrared-forbidden F_{2g} mode at 40 THz. (e) Transient
electric field and (f) intensity spectrum of a typical THz pump
pulse used in the experiments.

active [26–28]. The underlying symmetric C-C stretch
vibrations [Fig. 1(d)] are found in many other C-C cova-
lent-bond systems and were subject to several impulsive
SRS studies, for instance, on carbon nanotubes [29],
graphene [30], and organic molecules [31].

To drive and observe a 40 THz phonon, intense phase-
locked THz pump pulses and very short probe pulses are
required. The pump pulse is generated by difference-
frequency mixing of two phase-correlated infrared pulses
(energy 1.2 mJ, repetition rate 1 kHz) from two optical

parametric amplifiers in a GaSe crystal [25]. A typical
pump pulse and its intensity spectrum are shown in Figs. 1(e)
and 1(f), respectively. The CEP of the inherently phase-locked
pulse can be set by the delay between the two generating
infrared pulses [25]. The pump-induced coherent-phonon
dynamics are sampled by a synchronized ultrashort probe
pulse (duration 7 fs, center wavelength 750 nm) that measures
the transient birefringence of the sample [32]. Pump and probe
traverse the sample collinearly under normal incidence. Their
linear polarizations are set to an angle of 45° with respect to
each other. To obtain the pump electric field of Fig. 1(e), the
diamond sample is replaced by a GaSe crystal [25,33,34]. All
experiments are performed at room temperature and under
ambient conditions.

Coherent-phonon signals.—Figure 2 shows transient
optical birefringence signals $S(t)$ obtained for three differ-
ent center frequencies ω_0 of the pump pulse: Ω, $0.75\,\Omega$,
and $0.5\,\Omega$. When the pump center frequency is resonant with
the target mode [Fig. 2(a)], we observe a peak around $t = 0$,
whose shape approximately follows the intensity envelope
of the pump pulse [Fig. 2(b)]. It arises from the instantaneous
nonresonant response of the diamond electrons to the THz
pump pulse. Apart from this Kerr effect [35], however, we do
not observe any features indicative of a coherent lattice
vibration. When we lower the pump center frequency from
$\omega_0 = \Omega$ to $0.75\,\Omega$ [Fig. 2(c)], very similar dynamics are
found [Fig. 2(d)].

A strikingly different response is obtained when the
pump spectrum is centered at half the phonon frequency
[Fig. 2(e)]. For delays t larger than the pump-pulse duration,
the transient birefringence is dominated by an oscillatory
component [Fig. 2(f)] whose Fourier spectrum exhibits a
sharp peak at 40 THz [Fig. 2(e)]. By fitting an exponentially
damped harmonic oscillation to $S(t)$ for times $t > 200$ fs,
we obtain a center frequency of $\Omega/2\pi = 39.95$ THz and
damping constant of $\Gamma = 0.283$ ps^{-1} (see Fig. S1 of the
Supplemental Material [36]). These values agree excellently
with those inferred from SRS excitation using optical pump
pulses with a center frequency of 750 THz [26], as well as
from spontaneous Raman scattering [28] (also see Table S1
[36]). Therefore, the oscillatory pump-probe signal of
Fig. 2(f) is a clear hallmark of diamond's F_{2g} phonon. Its
decay is known to result from anharmonic interactions with
other lattice modes [28,44].

As seen in Fig. 3(a), the oscillation amplitude is found to
grow linearly with the pump power. Therefore, the
coherent lattice vibration is the result of two interactions
with the THz pump field [20] and can only arise from a
difference-frequency process [SRS, Fig. 1(b)] or a sum-
frequency process [SFE, Fig. 1(c)]. Since the coherent
phonon is only observed for a pump center frequency of
$\Omega/2$, we have provided evidence that we here observe a
coherent lattice vibration driven by SFE of a THz pulse.
Importantly, the transient signals do not exhibit any
indications of unwanted sample heating in the form of a
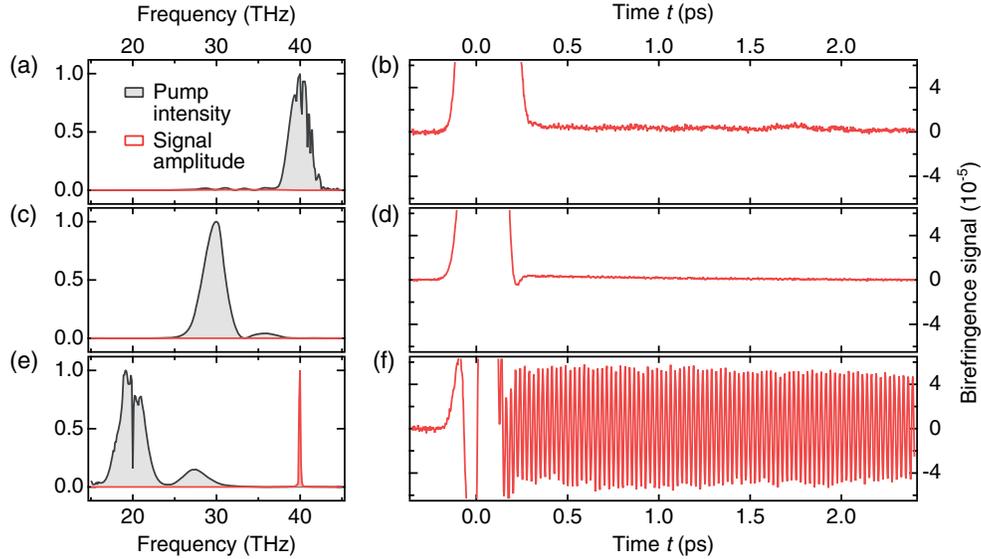
FIG. 2.   Sum-frequency excitation (SFE) of a coherent phonon. (a) Spectrum of a pump pulse centered at the phonon frequency $\Omega/2\pi \approx 40$ THz. (b) Resulting pump-probe signal, showing no signature of lattice vibrations. The peak around $t = 0$ is due to the instantaneous electronic response to the pump field. Panels (c),(d) and (e),(f) are as with (a),(b) but for a pump center frequency of 0.5 and 0.75 Ω, respectively. In panel (f), the long-lived oscillation reveals a coherent phonon at frequency $\Omega/2\pi \approx 40$ THz as seen in the signal spectrum of panel (e).

slowly varying background, as is often observed with optical excitation [4,5,15].

Model.—To put our interpretation on a theoretical basis, we assume that the solid has only one uniform vibrational mode, an optical phonon characterized by the normal coordinate Q and frequency Ω. The electric field $E(t)$ of the incident pump pulse exerts Coulomb forces on electrons and ions, resulting in a time-dependent electric-dipole density (polarization) $P(t)$. Since diamond is an insulator (electronic band gap 5.5 eV), the material remains in its electronic ground state whose electron density follows the pump field (photon energy ∼80 meV) adiabatically. Consequently, the polarization is fully determined by the instantaneous values of Q and E, and we have $P(t) = P(Q(t), E(t))$. We assume a Lagrangian [16] that captures the mode' s kinetic energy ($M\dot{Q}^2/2$), potential energy ($M\Omega^2 Q^2/2$), and interaction ($V_c PE$) with the pump field, where M is the effective mass of the lattice mode and V_c is the volume of diamond's unit cell. Linearizing P with respect to E and using the Lagrange equation yields the classical harmonic-oscillator-type equation of motion for Q,

$$\frac{M}{V_c}\left(\frac{\partial^2}{\partial t^2} + 2\Gamma\frac{\partial}{\partial t} + \Omega^2\right)Q = E\frac{\partial P}{\partial Q} + E^2\frac{\partial\chi}{\partial Q}, \quad (1)$$

which is also obtained by a quantum-mechanical treatment [15]. The right-hand side of Eq. (1) is the sum of two driving forces fully determined by the instantaneous value of $E(t)$. The first term describes the direct coupling of E to the polarization arising from lattice displacement. It corresponds to the 1PA scheme of Fig. 1(a), but vanishes here

because the effective charge $V_c\partial P/\partial Q$ of the infrared-inactive F_{2g} mode of diamond is zero. The second term results from the coupling of E to the Q-dependent part of the field-induced electronic polarization χE, where $\chi = \partial P/\partial E$ is the linear dielectric susceptibility. Clearly, this coupling is Raman-type because it is mediated by the Raman tensor $\partial\chi/\partial Q$, which is nonzero for the relevant mode [26,28].

Note that the second force term on the right-hand side of Eq. (1) follows the squared pump field $E^2(t)$. Therefore, it consists of a superposition of difference- and sum-frequency pairs of the spectrum of $E(t)$. The difference-frequency component, corresponding to conventional SRS [Fig. 1(b)], follows the pump intensity envelope. It has been employed for impulsive excitation of phonons [4,5,17] and magnons [3] in numerous works. As we show here, also the sum-frequency component is capable of driving such Raman-active modes [Fig. 1(c)]. It is precisely this term that describes phonon excitation by THz SFE.

As detailed in the Supplemental Material [36], we solve Eq. (1) for $Q(t)$ and model the transient optical birefrin-gence as a weighted sum of $Q(t)$ and $E^2(t)$, the latter capturing the instantaneous electronic response (THz Kerr effect [35]). A final temporal convolution with a square function accounts for the velocity mismatch of pump and probe pulses propagating through the sample [32]. Using this procedure and the actual driving field of Fig. 1(e), we obtain the gray line of Fig. 3(b). The agreement with the measured signal (blue line) is striking, in particular during temporal overlap of pump and probe pulses. Our model confirms that the sharp dip in the pump spectrum [Figs. 1(f)
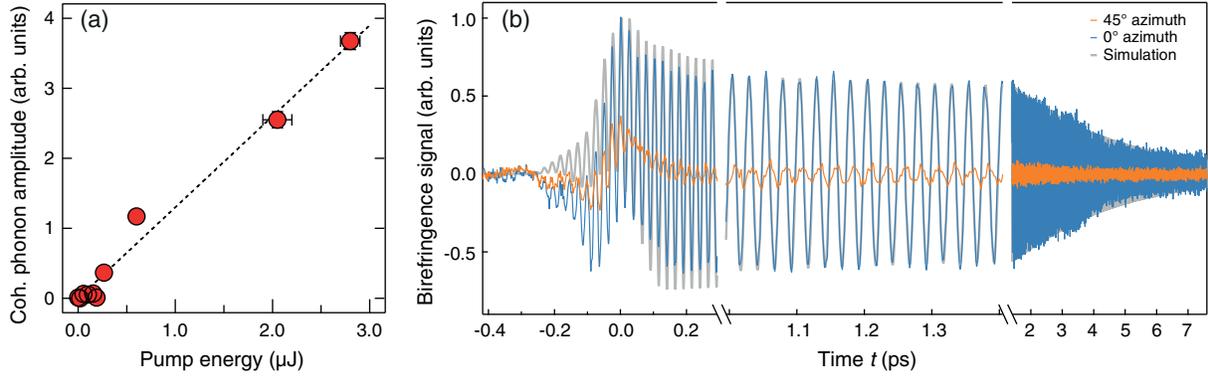
FIG. 3.   (a) Pump-energy dependence of the coherent phonon amplitude. (b) Measured (blue line) and simulated (gray line) THz-pulse-induced phonon dynamics [see Eq. (1) and text for model details]. Azimuthal sample rotation by 45° leads to an almost vanishing phonon signal (orange curve), consistent with the Raman-tensor symmetry of diamond [26]. The instantaneous electronic response ($t \approx 0$) is less prominent than in Fig. 2 since an optimized pump spectrum [Fig. 1(e)] was used (also see Supplemental Material [36]).

and 2(e)], which arises from absorption by CO_2 in ambient air, has negligible impact on the phonon dynamics [36].

The scaling of the pump-probe signal with the Raman tensor [see Eq. (1)] is consistent with its dependence on sample orientation [26,28]. For example, when the sample is rotated from the azimuth of largest phonon signal amplitude [blue line in Fig. 3(b)] by an angle of 45°, we find almost complete suppression of the oscillatory component [orange line in Fig. 3(b)], in agreement with the symmetry of the (100)-oriented diamond crystal [26]. Therefore, our results fully support the notion that we have observed THz SFE as a new mechanism for launching of a coherent phonon.

Coherent-phonon phase control.—Our experiment allows us to explore the impact of the CEP on the SFE process, which is expected to be very different from the SRS case. A CEP change by $\Delta\varphi_0$ shifts the phase of the phonon oscillation by $\Delta\varphi_0 - \Delta\varphi_0 = 0$ in the difference-frequency-type case [SRS, Fig. 1(b)], but by $\Delta\varphi_0 + \Delta\varphi_0 = 2\Delta\varphi_0$ in the sum-frequency process [SFE, Fig. 1(c)]. Unlike SRS, THz SFE should, therefore, enable direct phase control of coherent phonon motion by tuning the CEP of the pump pulse.

To put this expectation to test, we measure phonon dynamics as a function of the CEP as shown in Fig. 4. For example, when the CEP changes by $\Delta\varphi_0 = \pi/2$ [Fig. 4(a), green line], the phonon oscillation is found to undergo a phase shift of π [Fig. 4(b), green line]. The data of Figs. 4 and S2 of the Supplemental Material [36] demonstrate that twice the CEP shift of the pump field is directly transferred into the resulting lattice motion. These results and Eq. (1) highlight an interesting similarity to 1PA-driven dynamics, which are also sensitive to the pump CEP. Another common feature of the 1PA [Fig. 1(a)] and 2PA [Fig. 1(c)] scheme is that they permit nonimpulsive excitation with a pump pulse much longer than one phonon oscillation cycle.

Discussion.—Neither 2PA nor SFE have so far been observed for an optical transition between adjacent

vibrational levels. Here, we witness the full dynamics of this process, starting with the coherent SFE of the vibration, the subsequent decoherence and absorption. In contrast to previous quantum-coherent studies of 2PA by electronic transitions [23,24,45], the excited coherent-phonon state of this work has a much lower frequency and decoherence rate. Therefore, its dynamics can be sampled by a femtosecond optical probe directly in the time domain.

In terms of applications, the selective energy deposition in Raman-active modes by THz 2PA may enable machining of transparent materials by midinfrared industrial lasers. We estimate [36] that the 2PA strength by the diamond
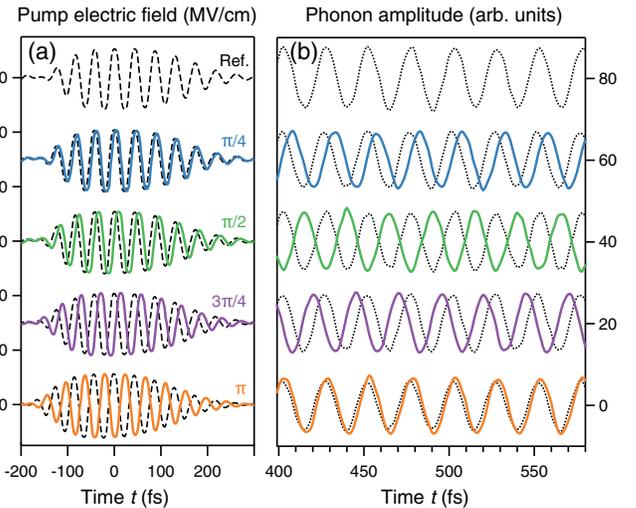
FIG. 4.   Demonstration of phonon phase control by tuning the CEP of the THz pump pulse. (a) Measured pump electric field for five CEP settings from 0 to π (solid lines). For comparison, the $\Delta\varphi_0 = 0$ reference transient (broken lines) is measured simultaneously for each CEP. (b) Resulting coherent phonon signals (solid lines) measured after sample excitation with the pump fields of panel (a) including reference phonon signals (broken lines).

phonon is only 1 order of magnitude smaller than that of strong optical two-photon absorbers such as GaAs or CdTe [46]. Moreover, THz SFE will potentially extend established, highly sensitive infrared vibrational spectroscopies to infrared-forbidden yet Raman-active modes. A prominent example is action spectroscopy [47], which relies on detecting modifications the absorbed infrared radiation has induced in the sample.

Remarkably, due to the low photon energies required, THz SFE provides a unique tool to steer chemical reactions [1] or phase transitions [7,8] in the electronic ground state, solely driven by Raman-active lattice vibrations. Shaping of THz pulses [48] to multicolor sequences could enable independent phase and amplitude control of the lattice trajectory along multiple normal coordinates, which is challenging with optical pulses accompanied by parasitic electronic excitations [49].

In conclusion, we have demonstrated that coherent lattice motion can be launched and controlled by THz SFE. This approach provides coherent control of all Raman-active modes that have so far been inaccessible by THz or mid-infrared radiation. Simultaneously, parasitic electronic excitation, which occurs when optical laser pulses are used, is greatly reduced. Finally, this so far neglected type of light-matter coupling extends infrared vibrational spectroscopy methods to infrared-forbidden modes.

---

*maehrlein@fhi-berlin.mpg.de

[1] J. L. LaRue, T. Katayama, A. Lindenberg, A. S. Fisher, H. Öström, A. Nilsson, and H. Ogasawara, THz-Pulse-Induced Selective Catalytic CO Oxidation on Ru, Phys. Rev. Lett. **115**, 036103 (2015).

[2] T. Kubacka *et al.*, Large-amplitude spin dynamics driven by a THz pulse in resonance with an electromagnon, Science **343**, 1333 (2014).

[3] A. V. Kimel, A. Kirilyuk, P. A. Usachev, R. V. Pisarev, A. M. Balbashov, and T. Rasing, Ultrafast non-thermal control of magnetization by instantaneous photomagnetic pulses, Nature (London) **435**, 655 (2005).

[4] T. K. Cheng, S. D. Brorson, A. S. Kazeroonian, J. S. Moodera, G. Dresselhaus, M. S. Dresselhaus, and E. P. Ippen, Impulsive excitation of coherent phonons observed in reflection in bismuth and antimony, Appl. Phys. Lett. **57**, 1004 (1990).

[5] G. C. Cho, W. Kütt, and H. Kurz, Subpicosecond time-resolved coherent-phonon oscillations in GaAs, Phys. Rev. Lett. **65**, 764 (1990).

[6] C. Klieber, E. Peronne, K. Katayama, J. Choi, M. Yamaguchi, T. Pezeril, and K. A. Nelson, Narrow-band acoustic attenuation measurements in vitreous silica at frequencies between 20 and 400 GHz, Appl. Phys. Lett. **98**, 211908 (2011).

[7] K. W. Kim, A. Pashkin, H. Schäfer, M. Beyer, M. Porer, T. Wolf, C. Bernhard, J. Demsar, R. Huber, and A. Leitenstorfer, Ultrafast transient generation of spin-density-wave order in the normal state of BaFe₂As₂ driven by coherent lattice vibrations, Nat. Mater. **11**, 497 (2012).

[8] M. Rini, R. Tobey, N. Dean, J. Itatani, Y. Tomioka, Y. Tokura, R. W. Schoenlein, and A. Cavalleri, Control of the electronic phase of a manganite by mode-selective vibrational excitation, Nature (London) **449**, 72 (2007).

[9] J.-W. Kim, M. Vomir, and J.-Y. Bigot, Ultrafast Magneto-acoustics in Nickel Films, Phys. Rev. Lett. **109**, 166601 (2012).

[10] T. Huber, M. Ranke, A. Ferrer, L. Huber, and S. L. Johnson, Coherent phonon spectroscopy of non-fully symmetric modes using resonant terahertz excitation, Appl. Phys. Lett. **107**, 091107 (2015).

[11] I. Katayama, H. Aoki, J. Takeda, H. Shimosato, M. Ashida, R. Kinjo, I. Kawayama, M. Tonouchi, M. Nagai, and K. Tanaka, Ferroelectric Soft Mode in a SrTiO₃ Thin Film Impulsively Driven to the Anharmonic Regime Using Intense Picosecond Terahertz Pulses, Phys. Rev. Lett. **108**, 097401 (2012).

[12] T. Qi, Y.-H. Shin, K.-L. Yeh, K. A. Nelson, and A. M. Rappe, Collective Coherent Control: Synchronization of Polarization in Ferroelectric PbTiO₃ by Shaped THz Fields, Phys. Rev. Lett. **102**, 247603 (2009).

[13] M. Jewariya, M. Nagai, and K. Tanaka, Ladder Climbing on the Anharmonic Intermolecular Potential in an Amino Acid Microcrystal via an Intense Monocycle Terahertz Pulse, Phys. Rev. Lett. **105**, 203003 (2010).

[14] R. Merlin, Generating coherent THz phonons with light pulses, Solid State Commun. **102**, 207 (1997).

[15] L. Dhar, J. A. Rogers, and K. A. Nelson, Time-resolved vibrational spectroscopy in the impulsive limit, Chem. Rev. **94**, 157 (1994).

[16] Y. R. Shen and N. Bloembergen, Theory of stimulated brillouin and raman scattering, Phys. Rev. **137**, A1787 (1965).

[17] E. M. Bothschafter, A. Paarmann, E. S. Zijlstra, N. Karpowicz, M. E. Garcia, R. Kienberger, and R. Ernstorfer, Ultrafast Evolution of the Excited-State Potential Energy Surface of TiO₂ Single Crystals Induced by Carrier Cooling, Phys. Rev. Lett. **110**, 067402 (2013).

[18] T. Dekorsy, G. C. Cho, and H. Kurz, in *Topics in Applied Physics*, edited by M. Cardona and G. Güntherodt (Springer, Berlin, Heidelberg, 2000), Vol. 76, p. 169.

[19] M. Foerst, C. Manzoni, S. Kaiser, Y. Tomioka, Y. Tokura, R. Merlin, and A. Cavalleri, Nonlinear phononics as an ultrafast route to lattice control, Nat. Phys. **7**, 854 (2011).

[20] S. Mukamel, *Principles of Nonlinear Optical Spectroscopy*, Oxford Series in Optical and Imaging Sciences, Vol. 6 (Oxford University Press, New York, 1999), Vol. 6.

[21] A. F. Gibson, C. B. Hatch, P. N. D. Maggs, D. R. Tilley, and A. C. Walker, Two-photon absorption in indium antimonide and germanium, J. Phys. C **9**, 3259 (1976).

[22] D. Seo, J. M. Gregory, L. C. Feldman, N. H. Tolk, and P. I. Cohen, Multiphoton absorption in germanium using pulsed infrared free-electron laser radiation, Phys. Rev. B **83**, 195203 (2011).

[23] D. Meshulach and Y. Silberberg, Coherent quantum control of two-photon transitions by a femtosecond laser pulse, Nature (London) **396**, 239 (1998).

[24] Y. Silberberg, Quantum coherent control for nonlinear spectroscopy and microscopy, Annu. Rev. Phys. Chem. **60**, 277 (2009).

[25] A. Sell, A. Leitenstorfer, and R. Huber, Phase-locked generation and field-resolved detection of widely tunable terahertz pulses with amplitudes exceeding 100 MV/cm, Opt. Lett. **33**, 2767 (2008).

[26] K. Ishioka, M. Hase, M. Kitajima, and H. Petek, Coherent optical phonons in diamond, Appl. Phys. Lett. **89**, 231916 (2006).

[27] C. V. Raman and K. S. Krishnan, A new type of secondary radiation, Nature (London) **121**, 501 (1928).

[28] S. A. Solin and A. K. Ramdas, Raman spectrum of diamond, Phys. Rev. B **1**, 1687 (1970).

[29] A. Gambetta, C. Manzoni, E. Menna, M. Meneghetti, G. Cerullo, G. Lanzani, S. Tretiak, A. Piryatinski, A. Saxena, R. L. Martin, and A. R. Bishop, Real-time observation of nonlinear coherent phonon dynamics in single-walled carbon nanotubes, Nat. Phys. **2**, 515 (2006).

[30] K. Ishioka, M. Hase, M. Kitajima, L. Wirtz, A. Rubio, and H. Petek, Ultrafast electron-phonon decoupling in graphite, Phys. Rev. B **77**, 121402 (2008).

[31] J.-Y. Bigot, T.-A. Pham, and T. Barisien, Femtosecond time resolved molecular dynamics of a polydiacetylene backbone, Chem. Phys. Lett. **259**, 469 (1996).

[32] M. Sajadi, M. Wolf, and T. Kampfrath, Terahertz-field-induced optical birefringence in common window and substrate materials, Opt. Express **23**, 28985 (2015).

[33] A. Leitenstorfer, S. Hunsche, J. Shah, M. C. Nuss, and W. H. Knox, Detectors and sources for ultrabroadband electro-optic sampling: Experiment and theory, Appl. Phys. Lett. **74**, 1516 (1999).

[34] Q. Wu, M. Litz, and X.-C. Zhang, Broadband detection capability of ZnTe electro-optic field detectors, Appl. Phys. Lett. **68**, 2924 (1996).

[35] M. C. Hoffmann, N. C. Brandt, H. Y. Hwang, K.-L. Yeh, and K. A. Nelson, Terahertz Kerr effect, Appl. Phys. Lett. **95**, 231105 (2009).

[36] See Supplemental Material at http://link.aps.org/supplemental/10.1103/PhysRevLett.119.127402 for model details and additional data, which includes Refs. [37–43].

[37] A. Schneider, I. Biaggio, and P. Günter, Terahertz-induced lensing and its use for the detection of terahertz pulses in a birefringent crystal, Appl. Phys. Lett. **84**, 2229 (2004).

[38] P. E. Martin and E. F. Barker, The infrared absorption spectrum of carbon dioxide, Phys. Rev. **41**, 291 (1932).

[39] W. B. Person and G. Zerbi, *Vibrational Intensities in Infrared and Raman Spectroscopy* (Elsevier Science Ltd., New York, 1982), Vol. 20.

[40] C. Kuebler, R. Huber, S. Tübel, and A. Leitenstorfer, Ultrabroadband detection of multi-terahertz field transients with GaSe electro-optic sensors: Approaching the near infrared, Appl. Phys. Lett. **85**, 3360 (2004).

[41] T. Kampfrath, J. Notzold, and M. Wolf, Sampling of broadband terahertz pulses with thick electro-optic crystals, Appl. Phys. Lett. **90**, 231113 (2007).

[42] R. W. Boyd, *Nonlinear Optics*, 3rd ed. (Academic, New York, 2008).

[43] M. D. Levenson, C. Flytzanis, and N. Bloembergen, Interference of resonant and nonresonant three-wave mixing in diamond, Phys. Rev. B **6**, 3962 (1972).

[44] P. G. Klemens, Anharmonic decay of optical phonon in diamond, Phys. Rev. B **11**, 3206 (1975).

[45] S. Zhang, H. Zhang, T. Jia, Z. Wang, and Z. Sun, Coherent control of two-photon transitions in a two-level system with broadband absorption, Phys. Rev. A **80**, 043402 (2009).

[46] J. H. Bechtel and W. L. Smith, Two-photon absorption in semiconductors with picosecond laser pulses, Phys. Rev. B **13**, 3515 (1976).

[47] J. Oomens, B. G. Sartakov, G. Meijer, and G. von Helden, Gas-phase infrared multiple photon dissociation spectroscopy of mass-selected molecular ions, Int. J. Mass Spectrom. **254**, 1 (2006).

[48] F. Eickemeyer, R. A. Kaindl, M. Woerner, T. Elsaesser, and A. M. Weiner, Controlled shaping of ultrafast electric field transients in the mid-infrared spectral range, Opt. Lett. **25**, 1472 (2000).

[49] H. Katsuki, J. C. Delagnes, K. Hosaka, K. Ishioka, H. Chiba, E. S. Zijlstra, M. E. Garcia, H. Takahashi, K. Watanabe, M. Kitajima, Y. Matsumoto, K. G. Nakamura, and K. Ohmori, All-optical control and visualization of ultrafast two-dimensional atomic motions in a single crystal of bismuth, Nat. Commun. **4**, 2801 (2013).